Maximum achievable aspect ratio in deep reactive ion etching of silicon due to aspect ratio dependent transport and the microloading effect

Junghoon Yeom, Yan Wu, John C. Selby, and Mark A. Shannon[a]
Department of Mechanical and Industrial Engineering, University of Illinois at Urbana-Champaign, 1206 West Green Street, Urbana, Illinois 61801

When etching high-aspect-ratio silicon features using deep reactive ion etching (DRIE), researchers find that there is a maximum achievable aspect ratio, which we define as the critical aspect ratio, of an etched silicon trench using a DRIE process. At this critical aspect ratio, the apparent etch rate (defined as the total depth etched divided by the total elapsed time) no longer monotonically decreases as the aspect ratio increases, but abruptly drops to zero. In this paper, we propose a theoretical model to predict the critical aspect ratio and reveal its causal mechanism. The model considers aspect ratio dependent transport mechanisms specific to each of the reactant species in the three subprocesses of a time-multiplexed etch cycle: deposition of a fluorocarbon passivation layer, etching of the fluorocarbon polymer at the bottom of the trench, and the subsequent etching of the underlying silicon. The model predicts that the critical aspect ratio is defined by the aspect ratio at which the polymer etch rate equals the product of the deposition rate and the set time ratio between the deposition and etching phases for the time-multiplexed process. Several DRIE experiments were performed to qualitatively validate the model. Both model simulations and experimental results demonstrate that the magnitude of the critical aspect ratio primarily depends on (i) the relative flux of neutral species at the trench opening, i.e., the microloading effect, and (ii) aspect ratio dependent transport of ions during the polymer etching subprocess of a DRIE cycle. © *2005 American Vacuum Society.* [DOI: 10.1116/1.2101678]

I. INTRODUCTION

Deep reactive ion etching (DRIE) of silicon has become a key process in the fabrication of microelectromechanical systems (MEMS). Many studies[1,2] have shown that there exists a maximum achievable aspect ratio, i.e., the critical aspect ratio, of silicon trenches etched by the DRIE process. Beyond this critical aspect ratio the apparent etch rate of a DRIE process (defined as the total depth etched divided by the total elapsed time) no longer monotonically decreases as aspect ratio increases, but abruptly drops to zero. The critical aspect ratio effectively constrains the design of high aspect ratio MEMS devices. A major challenge MEMS researchers face with DRIE technology is to understand the mechanism(s) governing the critical aspect ratio in order to maintain uniform etch rates over a larger range of aspect ratios and, ultimately, to extend the boundaries of the current design space for future generations of MEMS devices.

DRIE of silicon differs from conventional RIE technologies in that the technique utilizes a time-multiplexed inductively coupled plasma process (commonly known as the Bosch process) that employs two different plasma chemistries: an SF_6/Ar mixture for etching and a C_4F_8/Ar mixture for sidewall passivation. As shown in Fig. 1, one cycle of the DRIE process can be divided into three plasma subprocesses: (i) deposition of a fluorocarbon polymer passivation layer, (ii) etching of the fluorocarbon polymer at the bottom of the trench, and (iii) subsequent etching of the underlying silicon. The reactant species and transport phenomena associated with each DRIE subprocess are unique.

To date, many researchers have focused on the physics of reactant transport, when attempting to define the mechanisms giving rise to etch rate nonuniformities for various plasma etching processes.[1–5] With respect to the critical aspect ratio phenomenon in DRIE, aspect ratio dependent etching (ARDE) and the microloading effect have received some attention. ARDE is the phenomenon in which the apparent etch rate is inversely related to the aspect ratio of an evolving structural feature, in contrast to a length scale effect in which the apparent etch rate is proportional to the absolute size of an initial pattern feature. Gottscho *et al.*[5] suggested four possible mechanisms responsible for ARDE: (i) ion shadowing, (ii) differential charging, (iii) neutral shadowing, and (iv) Knudsen transport of neutrals. Several independent studies[1–4] on the ARDE effect in DRIE systems have shown that the apparent etch rate as a function of aspect ratio follows mostly the Knudsen transport model, also known as the flow conductance model, with a deviation seen in the high aspect ratio regime. At high aspect ratios, a "rollover" behavior is commonly observed, in which the apparent etch rate *decreases* with increasing etch time beyond the critical aspect ratio. Blauw *et al.*[1] suggested that the emergence of a maximum achievable aspect ratio was related to the reduced flux of etching species, the diminished removal of fluorocarbon polymer, and sidewall tapering at high aspect ratios. They used an ion-shadowing model to predict the aspect ratio associated with the onset of sidewall tapering. By increas-

[a]Author to whom correspondence should be addressed; electronic mail: mshannon@uiuc.edu

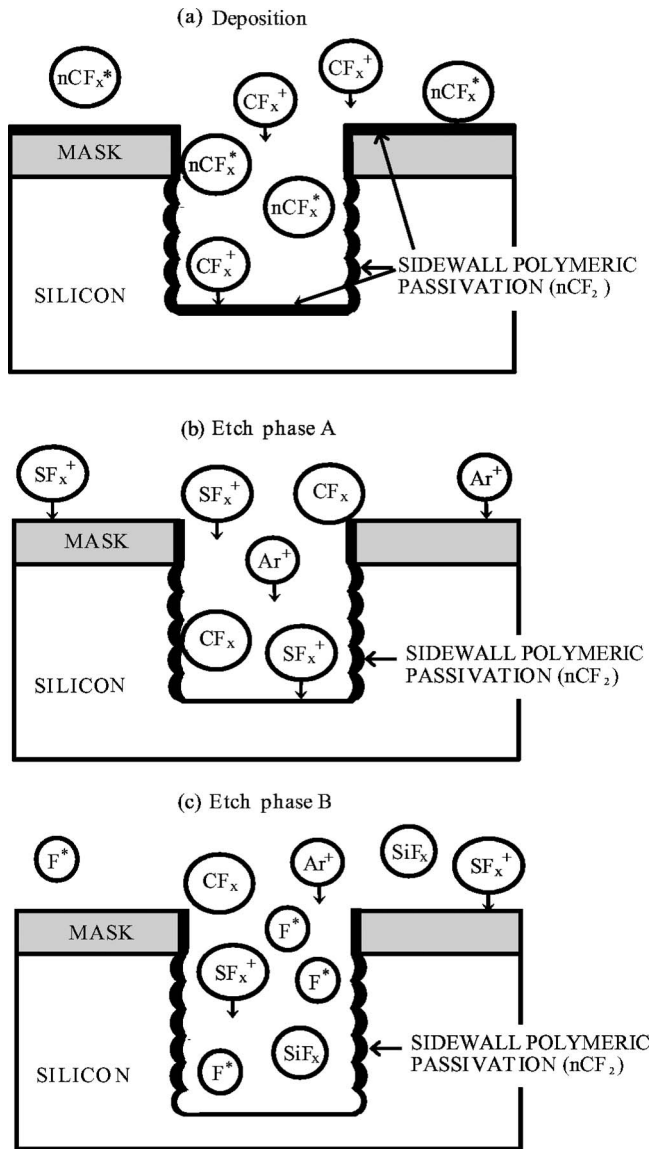**(a) Deposition**

(b) Etch phase A

(c) Etch phase B

FIG. 1. A diagram of a time multiplexed DRIE cycle: (a) deposition phase: isotropic deposition of a Teflonlike fluorocarbon polymer (nCF_2) passivation film; (b) etch phase: anisotropic etch of the passivation layer at the bottom of the trench; and (c) etch phase: isotropic etch of silicon with atomic fluorine. Ions and neutrals shown have crossed the sheath from the bulk plasma.

ing substrate rf bias during the etch subprocesses, they were able to increase the ion flux density at the bottom of developing trenches, which resulted in an increase in the observed maximum achievable aspect ratio. In our previous work,[2] we reported a critical aspect ratio dependence on the microloading effect, or a local dependence of etch rate on pattern area density. The closer etching patterns are packed together, and/or the greater the area to be etched in a given region, the slower the observed etch rate. In these experiments, increased microloading at a constant ion flux density led to smaller critical aspect ratios at which "rollover" was observed, implying that the depletion of the neutral reactant flux at the trench opening during DRIE also plays a meaningful role in determining the critical aspect ratio.
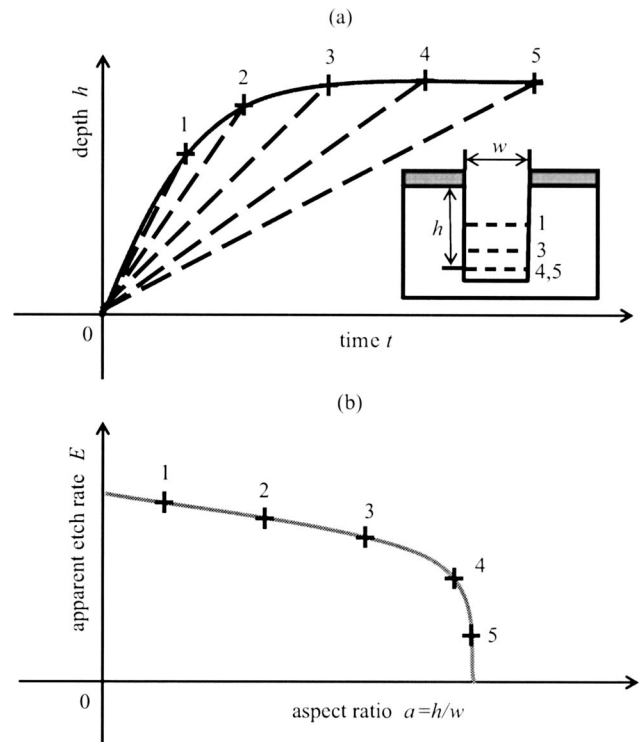

FIG. 2. Conceptual depiction of (a) the evolution of the depth, h, of a single silicon trench as a function of time, t, and (b) its corresponding apparent etch rate vs aspect ratio curve.

In this paper, a discrete one-dimensional model of the DRIE process is presented, i.e., a model that considers the etching of a silicon trench in a cycle by cycle manner. Specifically, the model breaks down a time-multiplexed DRIE cycle into three distinct subprocesses: fluorocarbon polymer deposition, passivation layer etching, and silicon etching. The aspect ratio dependent transport mechanisms of ions and neutrals unique to each subprocess are reviewed, and their individual contributions to the apparent etch rate of an evolving silicon trench are determined. The approach yields an analytical criterion governing the critical aspect ratio observed during a DRIE process. In order to explore the validity of the model, two controlled DRIE experiments will be presented in which changes in the critical aspect ratio were observed by varying either the pattern area density or the substrate bias voltage for a given etch process. Both effects are shown to be in qualitative agreement with the proposed model, in which the magnitude of the critical aspect ratio is a function of (i) the relative flux of neutral species at the trench opening, i.e., the microloading effect, and (ii) the aspect ratio dependent transport of ions during the DRIE process.

II. MODEL

Consider a conceptual experiment as shown in Fig. 2(a), following the evolution of a silicon trench during a DRIE process. The depth of an etched trench is plotted against the etching time in Fig. 2(a). As the elapsed etch time progresses from 1 to 3, the apparent etch rate, represented by the slopes of the dashed lines, gradually decreases to smaller and

smaller finite values. However, as etching progresses from 3 to 5, the instantaneous etch rate, the slope of the tangential line at each point in the solid curve, abruptly approaches a zero value, as the trench depth slowly reaches a plateau. The critical aspect ratio, or maximum achievable aspect ratio for a given trench size, is defined as the aspect ratio where the instantaneous etch rate identically equals zero. As the critical aspect ratio is approached asymptotically [Fig. 2(b), point 5], the depth of the trench increases very slowly, corresponding to the abrupt drop in the apparent etch rate versus aspect ratio curve. The apparent etch rate reaches a zero value only with infinite etching time.

A. Aspect ratio dependent reactant transport in a DRIE process

Now, consider a model of the conceptual DRIE experiment detailed above in which the etch progression is only a function of aspect ratio dependent reactant transport. Applying a single transport model to the entire DRIE process is not feasible because the mechanisms dominating the reactant transport for each of three subprocesses are not necessarily the same. None of the previously proposed transport models (Knudsen transport model, ion shadowing model, neutral shadowing model, etc.) by themselves exhibits the abrupt drop in apparent etch rate, or a critical aspect ratio phenomenon, in the high aspect ratio regime.

We view the apparent etch rate for a n cycle DRIE process as the total trench depth, h, divided by the total elapsed time, t. The trench depth, h, can be further broken down as the sum of an initial trench depth, $h_{initial}$, and the subsequent incremental etch progressions, H_k, occurring during each cycle k. Likewise, the etching time, t, can be expressed as the sum of an initial time lapse, $t_{initial}$, and the subsequent incremental times, T_k, elapsed during each cycle k. Furthermore, we partition the instantaneous etch rate of each cycle k into components corresponding to the three subprocesses of a time-multiplexed DRIE process. In this manner, we show how the aspect ratio dependent transport of each individual subprocess affects both the etch progression of a given cycle and the apparent etch rate of the overall process. The mathematical breakdown of the apparent etch rate model is detailed in the Appendix, and the relationship between apparent etch rate, instantaneous etch rate for a given cycle, and the dominant transport mechanisms of the three DRIE subprocesses is graphically illustrated in Fig. 3. Solid lines represent dominant relationships, and dashed lines show secondary effects. For instance, neutral species (e.g., $C_xF_y^*$) are central to the deposition of the fluorocarbon polymer passivation layer, while both neutrals (F^*) and ions ($Ar^+, S_xF_y^+$) are important in passivation layer etching (see Fig. 1). The mechanisms governing the reactant transport for each subprocess are based on archival literature. In the following sections, the primary mechanism for aspect ratio dependent reactant transport and the rational to neglect secondary effects will be discussed for each DRIE subprocess.
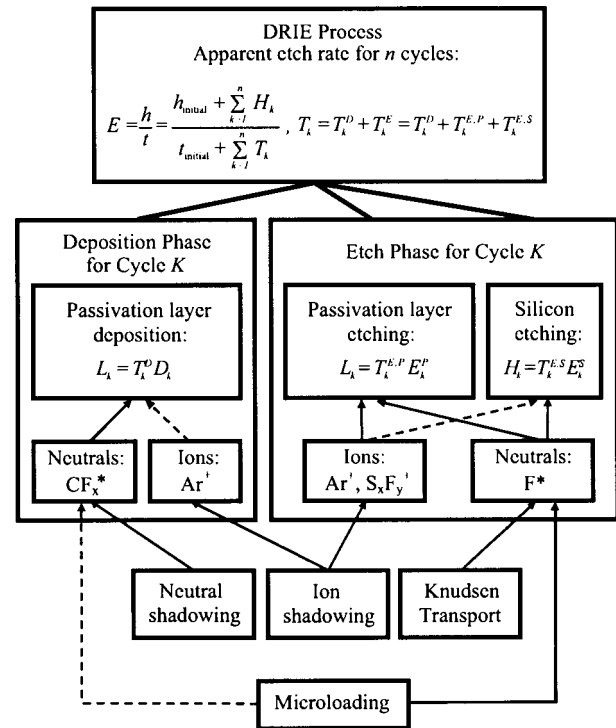

FIG. 3. A breakdown of the apparent etch rate observed for a DRIE process into a cycle by cycle etch progression, with each cycle partitioned into three subprocesses: (i) fluorocarbon polymer deposition, (ii) passivation layer removal, and (iii) silicon etching. The major reactants and transport mechanisms influencing each subprocess are indicated graphically. Solid lines indicate the dominant relations, and the dashed lines show secondary effects.

1. Deposition phase: Fluorocarbon polymer

In our ICP-DRIE system, we assume that the neutral flux density is the dominating factor in determining the polymer deposition rate and that the neutral shadowing model is appropriate to describe the transport of neutrals as a function of aspect ratio. In addition to direct deposition of neutral fluorocarbon radicals, Sowa *et al.*[6] pointed out that ion-assisted deposition potentially represents an equally dominant mechanism. However, we believe that the former is the dominant mechanism because the absence of the substrate bias during the deposition step would give rise to nonpreferential deposition covering of both sidewalls and the bottom of the etched structure. Thus, it is reasonable to neglect ion-assisted polymer deposition. Our observation also agrees with the investigation by Labelle *et al.*[7] on fluorocarbon film deposition from c-C_4F_8 plasmas for DRIE applications. They found that CF_2 radicals dominate only in high pressure/low power plasmas, in contrast to the low pressure/high power plasmas generated in our DRIE process.

A neutral shadowing model is appropriate to describe the transport of neutrals during the deposition phase, since it assumes a reaction probability of 1 for both the sidewalls and the bottom of an evolving trench. Measured deposition rates of fluorocarbon polymer as a function of aspect ratio by Schaepkens *et al.*[8] also support the use of a neutral shadow-

ing model. Based on the above arguments, we propose that the fluorocarbon polymer deposition rate for a given cycle k of a DRIE process can be expressed as[5]

$$D_k(a) = \frac{D(0)}{\sqrt{1 + 4a^2}}, \tag{1}$$

where a is the aspect ratio of the silicon trench (etched depth over trench width), and $D(0)$ is the deposition rate corresponding to an aspect ratio of zero. The magnitude of $D(0)$ depends on process parameters such as gas flow rate, chamber pressure, and coil power.

2. Etching phase: Silicon

A Knudsen transport model is used to determine the aspect ratio dependent silicon etch rate. It is widely accepted that in fluorine-based plasma etching of silicon, atomic fluorine reacts spontaneously with silicon and forms the volatile product, SiF_4.[9] With an applied substrate bias, the resulting ion bombardment enhances the etch rate of silicon by physical and chemical sputtering.[10] Questions arise as to whether the depletion of ions in the high aspect ratio regime should be taken into consideration when determining the aspect ratio dependence of silicon etching. By adding a spontaneous silicon etching term, Blauw *et al.*[11] developed a chemical enhanced ion-neutral synergy model for silicon etching in a SF_6-O_2 plasma. They found that in the limit of zero oxygen coverage, aspect ratio dependent etching based on the chemical enhanced ion-neutral model closely follows the Knudsen transport model which considered only the depletion of neutrals in the high aspect ratio regime. In our DRIE system, we do not use oxygen as an etch inhibitor, thus we argue it is reasonable to neglect the depletion of ions in the high aspect ratio regime.

The assumption of zero sidewall reaction probability represents a potential shortcoming of the Knudsen transport model when applied to the silicon etch subprocess of a DRIE cycle. It is known that some of the fluorine neutrals arriving at sidewalls either directly react with the fluorocarbon polymer or diffuse through the fluorocarbon polymer layer to react with the silicon underneath, thereby violating the assumption that the sidewall reaction probability is zero. However, the rates of both reactions at the sidewall are two orders of magnitude lower than the reaction rate of atomic fluorine with bare silicon at the bottom of the trench.[12] Thus, the Knudsen transport model is still a good approximation in describing the aspect ratio dependent transport of reactants for this subprocess. Results in several independent studies[1–4] on ARDE for the DRIE process also show that apparent etch rate as a function of aspect ratio closely resembles the Knudsen transport model. Based on the above arguments, we propose that the silicon etch rate for a given cycle k of a DRIE process can be expressed as[9]

$$E_k^S(a) = \frac{E^S(0)K(a)}{K(a) + S - K(a)S}, \tag{2}$$

where S is the reaction probability (or sticking coefficient) on the bottom of the trenches, $E^S(0)$ is the silicon etch rate

corresponding to an aspect ratio of zero, and $K(a)$ is the transmission probability as a function of aspect ratio. Methods of calculating $K(a)$ for cylindrical and rectangular structures have been studied in detail by Clausing.[13] In our model, we used the expression of $K(a)$ as derived for rectangular structures. In general, $E^S(0)$ is affected by the same process parameters as $D(0)$. However, $E^S(0)$ is also a function of the ion energy (as controlled by substrate bias). The impact of increased ion energy with higher substrate bias manifests in our model as a higher $E^S(0)$ value. Note that Eq. (2) neglects the role of ion angular distributions in determining the silicon etch rate.

3. Etching phase: Fluorocarbon polymer

An ion and neutral synergy model was selected to model the etching process observed during the removal of the fluorocarbon polymer passivation layer. Redeposition of nonvolatile etch products is also considered. Some studies on modeling trench evolution in a DRIE process attributed removal of the polymer layer solely to ion bombardment.[14,15] However, the importance of fluorine neutrals was also demonstrated by the fact that the etch rate of a fluorocarbon film by physical sputtering in an argon plasma is significantly lower than the etch rate observed with combined physical and chemical sputtering in a fluorocarbon plasma at similar ion current densities and ion energies.[12,16] Arguably, the combination of fluorine species and ion bombardment leads to a significant etch rate of fluorocarbon polymer. Thus, we argue that the ion-neutral synergy model is the most appropriate model for describing the polymer etching reaction. Mathematically, the ion-neutral synergy model at zero aspect ratio can be expressed as[5]

$$\mathrm{Syn}(0) = \frac{\nu S^N J^N}{1 + \dfrac{\nu S^N J^N}{\kappa E^I J^I}} = \frac{R^N(0)}{1 + \eta}, \tag{3}$$

where ν is the volume removed per reacting neutral (cm^3), S^N is the reactive sticking probability on a bare surface, and J^N is the neutral flux ($cm^{-2}\,s^{-1}$), κ is the volume of polymer removed per ion bombardment energy ($cm^3\,eV^{-1}$), E^I is the averaged ion energy (eV) (controlled by substrate bias), and J^I is the ion flux ($cm^{-2}\,s^{-1}$). We use the notation $R^N(0)$ to represent the combined term, $\nu S^N J^N$, at zero aspect ratio and η to represent the ratio, $\nu S^N J^N / \kappa E^I J^I$.

The aspect ratio dependence of ion transport is described by the ion-shadowing model with an assumed Gaussian ion angular distribution.[17] The transport of neutrals is governed by the neutral shadowing model. The ion-neutral synergy model at aspect ratio, a, can be expressed as

$$\mathrm{Syn}(a) = \frac{R_N(0)\Gamma^I(a)\Gamma^N(a)}{\Gamma^I(a) + \eta\Gamma^N(a)}, \tag{4}$$

where $\Gamma^I(a)$ and $\Gamma^N(a)$ are the flux ratios at the bottom of the trench with respect to the trench opening as a function of aspect ratio for ions and neutrals, respectively. An expression of $\Gamma^I(a)$ based on a Gaussian ion angular distribution is[17]

$$\Gamma^I(a) = \sqrt{\frac{2}{\pi\sigma}} \int_0^{\arctan(1/2a)} \exp\left(-\frac{\theta^2}{2\sigma^2}\right)d\theta, \tag{5}$$

where σ is the standard deviation of ion angles (controlled by substrate bias), which determines the broadness of the Gaussian distribution.

An expression of $\Gamma^N(a)$ based on an isotropic neutral angular distribution and a neutral shadowing model is[5]

$$\Gamma^N(a) = \frac{1}{\sqrt{1 + 4a^2}}. \tag{6}$$

Unlike the major etch product, SiF_4, produced during silicon etching, the etch products of fluorocarbon polymer etching, specifically fluorocarbon monomers, are less volatile and can potentially be redeposited on the sidewalls as well as the bottom of the trench during DRIE.[16,18] In our system, we speculate that the redeposition of the etch products of the fluorocarbon polymer increasingly hinders the polymer etching at the bottom of the trench as the aspect ratio increases. Research by Cho *et al.*[19] showed that significant sidewall etching occurs once a sidewall is no longer perpendicular to the bottom surface of the trench, i.e., when tapering starts. We propose that the etching of a tapered sidewall leads to enhanced redeposition of the etched products on the trench bottom, giving rise to an observed decrease in the polymer etch rate from what would be expected at that same aspect ratio in the absence of polymer redeposition. Additionally, material derived from the trench bottom that redeposits on the sidewall can further increases the angle of taper that will affect the subsequent etch cycle. To account for redeposition of fluorocarbon polymer and a corresponding reduction in passivation layer etch rate, an aspect ratio dependent knock-down factor, taking the mathematical form of exponential function, is introduced into our overall polymer etch rate model. Based on Eqs. (3)–(6), the proposed expression for the polymer etch rate for a given cycle k of a DRIE process becomes

$$E_k^P(a) = \frac{R_N(0)\Gamma^I(a)\Gamma^N(a)}{\Gamma^I(a) + \eta\Gamma^N(a)} \exp\left(-\frac{a}{A_{\text{taper}}}\right). \tag{7}$$

The scaling constant, A_{taper}, is the aspect ratio at which the onset of measurable tapering occurs, which can be determined from SEM images of silicon trenches etched in a DRIE process. When sidewall profiles were approximated using a trapezoidal form as seen, in the inset of Fig. 4, A_{taper}, defined as h_{taper}/w, was found to range from 10 to 15. For modeling purposes, we assumed A_{taper} to be a constant; its dependence on parameters such as microloading and substrate bias needs further study.

B. Modeling the microloading effect

Few efforts have been made to model the microloading effect[20–22] in a DRIE process. While ions are primarily driven to the substrate by the electric field, neutrals reach the substrate by diffusion. For etch processes involving neutrals, the governing reaction is often transport limited as opposed
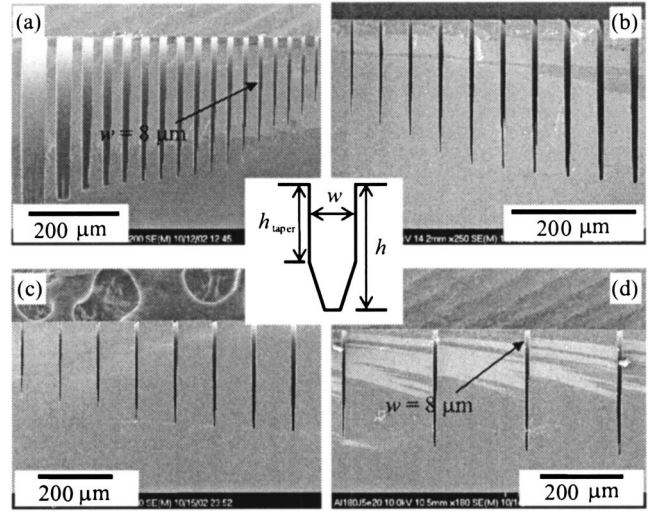

FIG. 4. SEM images of silicon trenches evolving from four different initial pattern area densities, etched in a 3 h ICP-DRIE process: (a) 80% microloading with 25 μm line spacing, (b) 50% microloading with 50 μm line spacing, (c) 30% microloading with 100 μm line spacing, and (d) 10% microloading with 200 μm line spacing.

to rate limited. The diffusion limitation of neutrals between the plasma discharge and the substrate leads to spatial variations of neutral concentration and thus etch rates that are dependent on local pattern area density. While microloading can happen in both the deposition and etching subprocesses of DRIE, the depletion of excited fluorine neutral concentrations during the etching phase is usually responsible for the microloading effect.[23]

In our model, a pattern density dependent etch rate is accounted for by introducing a loading factor, L, that normalizes the neutral flux at the trench opening for both silicon and fluorocarbon polymer etching with respect to a model pattern area density of 10%, or 0.1 mm^2/mm^2. With this normalization, L can theoretically range from zero to infinity, but for our DRIE experiments, L falls in the range of 0–1. The loading factor, L, is inversely proportional to pattern density, thus directly proportional to etch rate. Introducing the loading factor concept into Eqs. (2) and (7), the expressions for silicon etch rate and fluorocarbon polymer etch rate, respectively, for the kth cycle of a DRIE process become

$$E_k^S(a) = \frac{E^S(0)K(a)L}{K(a) + S - K(a)S} \tag{8}$$

and

$$E_k^P(a) = \frac{R_N(0)\Gamma^I(a)\Gamma^N(a)L}{\Gamma^I(a) + \eta\Gamma^N(a)L} \exp\left(-\frac{a}{A_{\text{taper}}}\right). \tag{9}$$

C. Simulations

Model simulations of a time-multiplexed DRIE process were performed to predict the apparent etch rate as a function of aspect ratio during the evolution of a silicon trench. A flow chart of the simulation is depicted in Fig. 5. Initial conditions for each model simulation were configured with
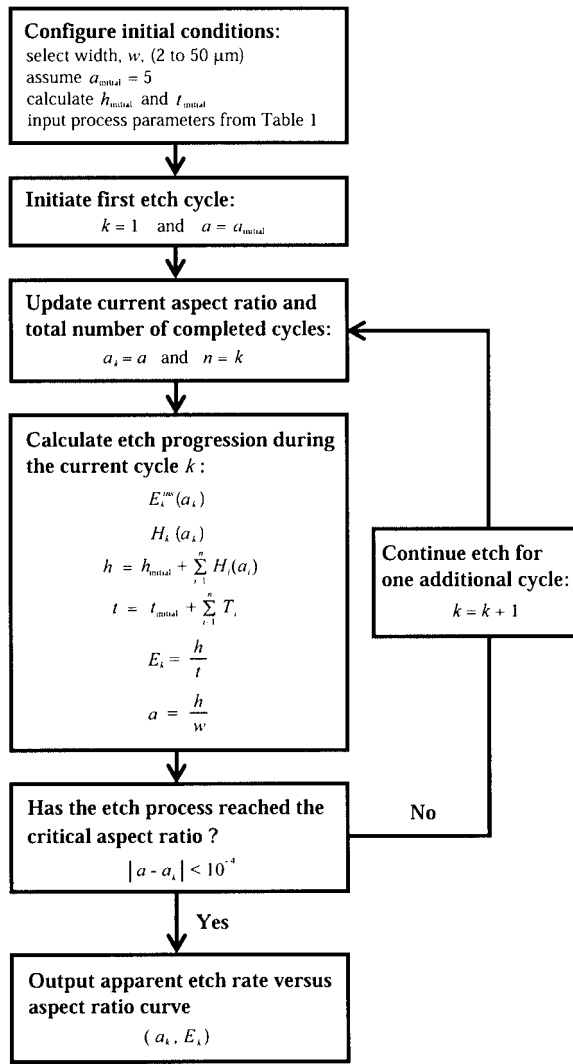
FIG. 5. A flow chart of the model simulation. Refer to the text for the detailed description.

TABLE I. Model fitting parameters.

Substrate bias level	A (low)		B (high)
$E^S(0)$[a]	5.9 μm/min		6.1 μm/min
S[a]	0.40		0.40
$D(0)$[b]	0.09 μm/min		0.09 μm/min
σ[c]	0.174 rad		0.087 rad
A_{taper}[d]	14	12, 14	14
β[d]	0.7		0.7
T[d]	16.7 s		16.7 s
$E_{initial}$[d]	2.10 μm/min	1.95 μm/min	2.35 μm/min
$E(0)$[d]	2.40 μm/min	2.24 μm/min	2.80 μm/min
L[e]	1	0.94	1
$R^N(0)$[e]	1.02 μm/min		1.02 μm/min
η[e]	4.5		3

[a]Reference 11.
[b]Reference 7.
[c]Reference 17.
[d]Parameters adapted from the experimental input or observation.
[e]Fitted parameters.

$$E(0) = \frac{1}{(1 + \beta)}\left(1 - \frac{\beta D(0)}{E^P(0)}\right)E^S(0), \tag{10}$$

where

$$E^P(0) = \frac{R^N(0)}{1 + \eta}. \tag{11}$$

With $E^S(0)$, $D(0)$, and β fixed, we estimated $R^N(0)$ and η subject to the constraint that $E(0)$, calculated with Eqs. (10) and (11), match the apparent etch rate at zero aspect ratio for the given data set. DRIE subprocess parameters were assumed constant for all cycles, i.e., $\beta_k = \beta =$ constant, $T_k = T$ = constant, etc. All parameters used in the DRIE simulations are listed in Table I.

After configuration of the initial conditions, each simulation was conducted as follows. Using the assumed values for the various sub-process parameters, we calculated the instantaneous etch rate for the first cycle, $E_1^{ins}(a_1 = a_{initial} = 5)$, using Eq. (A8). Next, we calculated the incremental etch progression for the first cycle, H_1, using Eq. (A7), given the time elapsed T_1. Adding H_1 to $h_{initial}$, and adding T_1 to $t_{initial}$, we then calculated the apparent etch rate corresponding the first etch cycle, E_1, as given by Eq. (A11). Now, the aspect ratio observed at the beginning of the second cycle, a_2, was calculated, followed by evaluation of H_2 and then E_2. This sequence of calculations was repeated in a cycle by cycle manner until sequential values of a_k agreed to within four decimal places at which point the simulation was terminated. Two different substrate bias levels were simulated, representing two electrode power settings during the etching phase. For the lower bias level, the DRIE process was also simulated with two different microloading levels. Simulation results are discussed in conjunction with the experimental results included in Sec. IV.

low aspect ratio etch data ($a < 5$) from a given set of experimental data as follows. First, a trench width, w, was assumed (2–50 μm wide), and an initial trench depth, $h_{initial}$, was calculated based on an assumed initial aspect ratio, $a_{initial} = 5$. A time lapse, $t_{initial}$, was then selected such that the initial apparent etch rate, $E_{initial}$, matched the apparent etch rate observed for $a = 5$ in the corresponding data set. Next, a value for the cycle period, T_k, was selected, as well as the set time ratio between the deposition and etching phases, β_k. Simulation parameters $D(0)$, S, and $E^S(0)$ in Eqs. (1) and (8) were selected to be similar to previously published values for their respective subprocesses. Due to the lack of literature in fluorocarbon polymer etching, parameters in Eq. (9) were chosen to reflect that when substrate bias changes from low to high, $R^N(0)$ is unaffected, η decreases due to the higher ion bombardment energy, and σ deceases due to a more narrow ion angular distribution. The apparent etch rate at zero aspect ratio, or equivalently stated, the initial instantaneous etch rate of the DRIE process, can be written as

III. EXPERIMENT

In order to explore the validity of the model, two separate DRIE experiments were performed to observe changes in the critical aspect ratio as a function of (i) pattern area density or (ii) the substrate bias voltage for a given etch process. Pattern area density represents an experimental variable that allows one to indirectly control the relative flux of neutral species at the trench opening during a DRIE process. In other words, pattern area density provides control of the microloading effect. Often, as in our case, an inductively coupled plasma is created from a gas mixture, and depending on the subprocess, a separate rf bias can be applied to the substrate being etched in order to adjust the directionality of ion flux towards the substrate. By adjusting the substrate bias voltage, one can indirectly control the aspect ratio dependent transport of ions during the DRIE process. With respect to our model, a change in pattern density is reflected by a change in the loading factor, L, for the silicon and fluorocarbon polymer etch subprocesses. A change in substrate bias voltage is reflected by a change in $E^S(0)$ during the silicon etch subprocess as well as changes in η (via a change in E^I) and σ during the fluorocarbon polymer etch subprocess.

A brief outline of the experimental design and wafer fabrication procedure is described below, and a detailed description can be found elsewhere.[2] Each test wafer was designed with four different zones of pattern area density, each incorporating rectangular lines 10 mm long, with widths ranging from 3 to 1000 μm. These dimensions were selected so that the transmission probability, $K(a)$, for a long slit feature[13] could be used in our model simulations. In each patterned area, lines were equally separated with a spacing parameter to control the microloading effect. The spacing between the lines in the four patterns was 25, 50, 100, and 200 μm, respectively. To amplify the microloading effect, different sizes of "dummy" loading areas were added to each of the four test patterns. For the pattern with 25 μm line spacing, approximately 80% of the die area was covered with bare silicon, including the pattern itself. Similarly, the pattern with 50 μm line spacing had 50% loading, the 100 μm line spacing pattern had 30% loading, and the 200 μm line spacing pattern contained no "dummy" region, effectively resulting in a 10% loading pattern.

Each test wafer was fabricated as follows. A layer of 1000 Å thick aluminum film was sputtered on an *n*-type lightly doped silicon wafer to serve as etching mask. The pattern was transferred to the aluminum film by a lift-off process. The wafer was then etched in an inductively coupled plasma etcher for 180 min using a time-multiplexed DRIE process with SF$_6$ for etching and C$_4$F$_8$ for sidewall passivation. The processing parameters used throughout this work, listed in Table II, were optimized to yield silicon trenches with vertical sidewall profiles. The dimensions (and therefore aspect ratios) of all etched silicon trenches were measured with Hitachi S-4700 high resolution scanning electron microscopy (SEM). Although our model is based on the conceptual experiment of tracking the etch progression of a single silicon trench over a large span of elapsed times, the

TABLE II. Process parameters.

Parameters	Deposition	Etching
Process time	5 s	7 s
SF$_6$ flow rate	1 sccm	100 sccm
C$_4$F$_8$ flow rate	70 sccm	4 sccm
Ar flow rate	40 sccm	40 sccm
Electrode power	0	6 or 8 W
Coil power	850 W	850 W
Chamber pressure	22 mTorr	24 mTorr

aspect ratio dependent etching experiments were conducted by etching trenches with different widths for a single etching time due to the destructive nature of the SEM measurement.

IV. RESULTS AND DISCUSSION

Sample SEM images of experimentally etched trench profiles shown in Fig. 4 illustrate the phenomenon of a critical aspect ratio. As the aspect ratio of a silicon trench increases beyond an aspect ratio ranging from 10 to 15, trench sidewalls become tapered. As the sidewalls further taper to a tip (see the trenches with smaller opening sizes), etching completely stops at the critical aspect ratio. In our model, the maximum achievable aspect ratio for a given trench width is analytically defined as the aspect ratio at which the instantaneous etch rate of a given cycle in the DRIE process reaches zero. At this critical aspect ratio, the depth of the trench reaches a plateau. With continued etching, the apparent etch rate will slowly approach a zero value. The model simulation, specifically Eq. (A8), provides a criterion for the critical aspect ratio, a_k, in which

$$\beta_k D_k(a_k) = E_k^P(a_k). \tag{12}$$

Physically, this condition occurs when all the time in etching phase, T_k^E, is devoted to fluorocarbon polymer etching, and the underlying silicon cannot be exposed for etching to proceed. For the model simulations, silicon etching slows exponentially as the aspect ratio of the trench approaches the critical aspect ratio, and a zero instantaneous etch rate is approached asymptotically.

Graphically, if we plot $\beta D(a)$ and $E^P(a)$, as shown in Fig. 6, we find that the critical aspect ratio can be determined from the crossing point of the two curves. For a given process where β is assumed to be the lone control variable, decreasing β may result in a higher critical aspect ratio, as shown in Fig. 6. Under a given set of process conditions, $E^P(a)$ asymptotically approaches zero at an infinite aspect ratio, and therefore it is theoretically possible to increase, without limit, the observed critical aspect ratio by decreasing β to smaller and smaller values. However, for real ICP-DRIE systems, the etch rate of the fluorocarbon polymer will reduce to a negligible value at a finite aspect ratio, and etching will cease because the underlying silicon cannot be exposed. This aspect ratio represents an absolute limitation of the maximum achievable aspect ratio, depicted as a^* in Fig. 6. Practically, extending the critical aspect ratio by adjusting
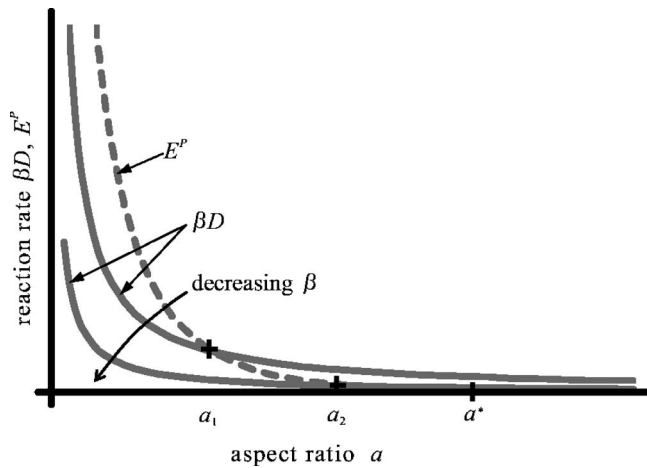
FIG. 6. Diagram illustrates the criterion of zero instantaneous etch rate, as given by Eq. (12), demonstrating that the crossing point of the βD vs a and E^P vs a curves determines the critical aspect ratio of a DRIE process.

the β value will be further constrained by the sidewall profile requirements of the given etching application and cannot be changed arbitrarily.

In developing the model simulation, we noted that with typical values of $D(0)$ and $E^P(0)$, the initially proposed ion and neutral synergy model for etching of the fluorocarbon polymer, as given by Eq. (4), exhibited a higher reaction rate than the neutral shadowing model for deposition of the passivation layer, as given by Eq. (1), for all aspect ratios. As a consequence, these simulations did *not* predict a critical aspect ratio phenomenon. After careful review of current literature, it was postulated that redeposition of the fluorocarbon passivation layer on the bottom of the trench during the polymer etch subprocess must be effectively reducing the etch rate from the value predicted when considering only the transport of reactant species. Furthermore, it was noted that polymer redeposition could possibly be dependent on the angle of sidewall taper.[19] We noted in our DRIE experiments that sidewall tapering was a strong function of aspect ratio. When viewed in context, these observations provided the phenomenological basis for the aspect ratio dependent exponential knock-down factor and the physical constant, A_{taper}, that were introduced to the polymer etch model in Eqs. (7) and (9).

In subsequent paragraphs, etch simulations of apparent etch rate versus aspect ratio curves will be compared to experimental data. For clarity, it is important to note that the apparent etch rate versus aspect ratio curve generated by a model simulation for a given set of DRIE process parameters is *independent* of the initial trench width, w, selected during model configuration. This outcome is expected, due to the fact that the model considers only the physics of *aspect ratio* dependent transport and not length scale effects. However, the total number of process cycles and hence the total etching time required to reach the critical aspect ratio is *dependent* on w.

In our first experiment, we explored the dependence of critical aspect ratio on the microloading effect. Etching pro-
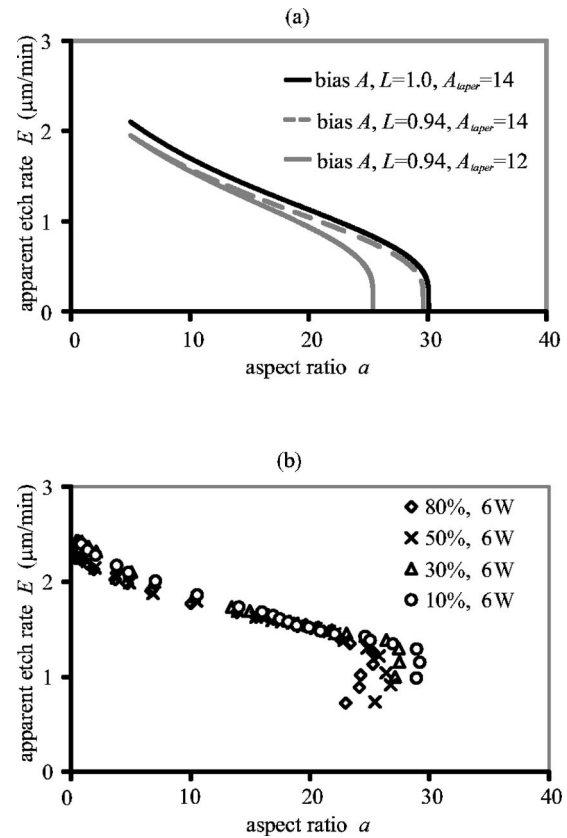

FIG. 7. (a) Model predictions and (b) experimental results for a DRIE process with constant bias level and variable microloading. Critical aspect ratio *decreases* with *increased microloading* resulting from an increase in pattern area density. The decrease in critical aspect ratio observed in simulation results becomes more pronounced if A_{taper} is assumed to decrease with increased microloading.

files for trenches originating from the largest relative pattern area density, Fig. 4(a), exhibit more pronounced tapering compared to trenches involving in the presence of a decreased microloading effect, Fig. 4(d). For instance, compare the trenches with $w=8$ μm in Figs. 4(a) and 4(d). The 8 μm trench evolving in the presence of an increased microloading effect, Fig. 4(a), has terminated in a tapered tip, whereas the 8 μm trench evolving in the presence of a relatively decreased microloading effect, Fig. 4(d), has not quite reached its critical aspect ratio. These observations are related to the critical aspect ratios found in the apparent etch rate versus aspect ratio curves shown in Fig. 7. With the same substrate bias (6 W), an increased microloading effect leads to a smaller critical aspect ratio. As can be seen in Fig. 7(a), model simulations with two different loading factors and the same substrate bias level qualitatively show the same critical aspect ratio dependence on microloading as observed in the experimental data. In both Figs. 7(a) and 7(b), an increased microloading effect leads to a decrease in the observed critical aspect ratio. Additionally, the simulation also shows that a relative decrease in the microloading effect results in overall upward vertical shift in the apparent etch rate versus aspect ratio curve, a trend that is also evident in the data. The dependence of the critical aspect ratio on the microloading

effect can be explained using Eqs. (9) and (12). In Eq. (9), decreasing L (while keeping all other parameters constant) results in a smaller $E_k^P(a)$ value for a given aspect ratio a, which means that an increased microloading effect leads to a smaller passivation layer etch rate. Consequently, the criterion for determining the critical aspect ratio, Eq. (12), is satisfied at a smaller aspect ratio because the polymer deposition rate is unaffected by microloading conditions.

As a final note on the microloading effect, we point out that for the same increase in pattern area density, a much smaller critical aspect ratio was observed in the experimental data, relative to the value of the critical aspect ratio predicted by the simulation. To explain this discrepancy, we hypothesized that A_{taper} is a function of pattern area density and is not *independent* of the microloading effect as we had previously assumed in our simulations. After a careful examination of our SEM images, we concluded that an increase in microloading can be correlated to a decrease in A_{taper}. At this time, we do not have enough data to postulate on the physical mechanisms underlying this observed trend. However, if we allow A_{taper} to decrease as microloading increases in our model simulation [Fig. 7(a)], a smaller critical aspect ratio is predicted, better resembling the microloading effect observed in our experimental data.

In a second experiment, we compared the apparent etch rates of silicon trenches etched under identical microloading conditions but with different levels of substrate bias. In our ICP-DRIE system, substrate bias is adjusted by applying a different electrode power. The apparent etch rate versus aspect ratio curves for two substrate bias levels, corresponding to 6 W and 8 W of electrode power, are plotted in Fig. 8(b). Also note the two different microloading conditions. As electrode power was increased from 6 W to 8 W, the critical aspect ratio increased from 26 to 35 for the trenches evolving from an initial pattern area density of 80%, and from 29 to 38 for trenches evolving from an initial pattern area density of 10%. Model simulations predict the same critical aspect ratio dependence on substrate bias level, as shown in Fig. 8(a). Additionally, model simulations predict an upward vertical shift in the apparent etch rate versus aspect ratio curve associated with increased substrate bias, a trend also observed in the data. A higher bias level leads to a decrease of η and an increase in $\Gamma^I(a)$ in Eq. (9) due to an increase in ion bombardment energy and a narrower ion angular distribution. Both decreasing η and increasing $\Gamma^I(a)$ leads to a higher passivation layer etch rate, $E^P(a)$, for a given aspect ratio and level of microloading. As a consequence, the critical aspect ratio criterion, as given in Eq. (12), is satisfied at a higher aspect ratio because the deposition subprocess is unaffected by substrate bias level settings.

A critical review of our experimental results reveals several limitations of our model. First, and foremost, the model is one-dimensional; it does not account for changes in sidewall profile as a function of aspect ratio, i.e., the model does not predict the trench tapering observed in our data. A two-dimensional model that accounts for sidewall tapering could more closely approximate the physics of the aspect ratio de-
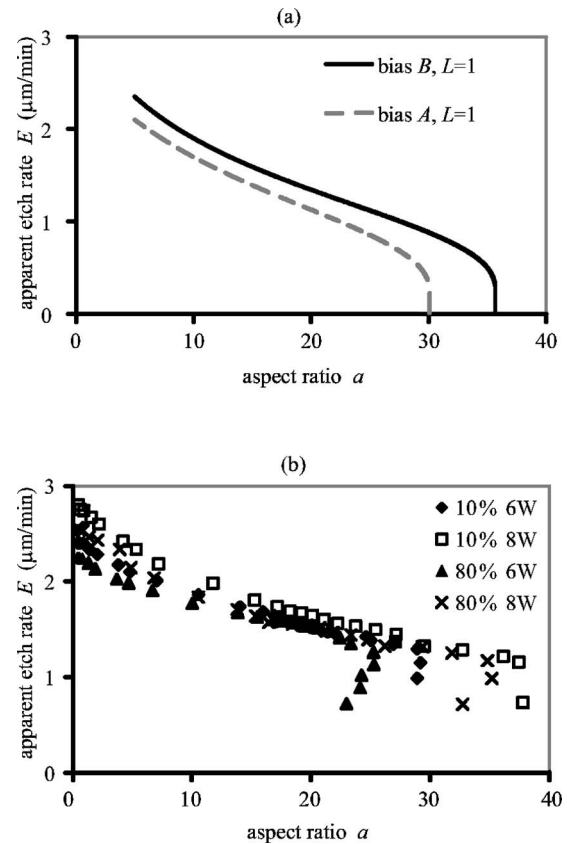

FIG. 8. (a) Model predictions and (b) experimental results for a DRIE process with constant microloading and variable bias level. Critical aspect ratio *increases* with *increased bias level* during the etch phase of the DRIE process.

pendent transport evolving during the DRIE process and thus provide a more accurate determination of the critical aspect ratio. Secondly, although the model indeed demonstrates an aspect ratio limitation in the form of an abrupt drop in apparent etch rate, it does not show the "rollover" behavior observed in the data in which the apparent etch rate *decreases* with increasing etch time after the critical aspect ratio has been reached. However, it is important to note that the experimental data was collected by etching trenches with different initial widths for a single etching time, while our model predicts a temporal progression of the etching of a *single* trench. Consider, for example, the construction of the apparent etch rate versus aspect ratio curve for the data collected from the 80% pattern area density and 6 W substrate bias experiment, as shown in Fig. 8. Each data point was derived from the etching of a trench with a different initial width. With a closer look at the data points in the "rollover" regime, we note that each point represents etch data from sequentially increasing trench widths, as shown in Fig. 9, which may suggest that the apparent etch rate in this high aspect ratio regime is a function not only of aspect ratio but also of the absolute trench width.[5] Additionally, we did not take into account sidewall profile when calculating the aspect ratio of a given trench, but rather calculated the aspect ratio simply as h/w (see Fig. 4). In reality, the contribution of
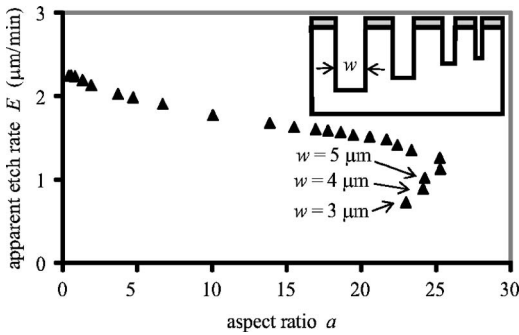
FIG. 9. An example of the apparent etch rate vs aspect ratio curve from experimental data showing "rollover" behavior in the high aspect ratio regime and the possibility of length scale effects on the rollover points.

lateral sidewall etching to the measured aspect ratio may not be neglected when the absolute feature size of a given trench is small, i.e., less than 5 μm. Further study is needed to investigate the effect(s) of absolute trench size or length scale on apparent etch rate and the critical aspect ratio phenomenon.

V. CONCLUSIONS

We have developed a one-dimensional model for cycle by cycle etch progression in a DRIE process. In this model, we have partitioned each individual cycle of a time-multiplexed DRIE process into components corresponding to its three basic subprocesses to show how aspect ratio dependent reactant transport affects both the instantaneous etch rate of a given cycle and the apparent etch rate of the overall process. As a result, the model provides an analytical criterion for the maximum achievable aspect ratio, or critical aspect ratio, observed in a DRIE process: the aspect ratio at which the instantaneous polymer etch rate equals the product of the instantaneous deposition rate and the set time ratio between the deposition and etching phases. Consequently, the transport mechanisms that dominate the relative rates of these two specific DRIE subprocesses must govern the critical aspect ratio phenomenon. Finally, by varying pattern area density and substrate bias levels in both experiments and model simulations, we conclude that the magnitude of the critical aspect ratio can be controlled by (i) the relative flux of neutral species at the trench opening, i.e., the microloading effect, and (ii) the aspect ratio dependent transport of ions during the polymer etching subprocess of a DRIE cycle.

APPENDIX

Assume that a silicon trench of a given width, w, has been etched with a DRIE process to an initial depth, h_{initial}, during an elapsed time, t_{initial}, such that $h_{\text{initial}}/w = a_{\text{initial}} = 5$. For this initial aspect ratio, the initial apparent etch rate, E_{initial}, can be estimated as

$$E_{\text{initial}} = \frac{h_{\text{initial}}}{t_{\text{initial}}}. \tag{A1}$$

Now, after n additional cycles of the DRIE process, the trench will be etched to a depth, h, during a total elapsed time, t. The apparent etch rate after n additional cycles of etching can be written as

$$E_n = \frac{h}{t}. \tag{A2}$$

If the time period of etching a given cycle, k, during the DRIE process is T_k, the total elapsed time of the DRIE process can be written as

$$t = t_{\text{initial}} + \sum_{k=1}^{n} T_k = t_{\text{initial}} + \sum_{k=1}^{n} T_k^D + \sum_{k=1}^{n} T_k^E, \tag{A3}$$

where T_k^D and T_k^E are the time spent in the deposition phase and etching phase of the kth cycle, respectively. In a time-multiplexed DRIE process, different gases and substrate biases are used for the deposition and etching phases, and the times set for each phase are independently controlled by the operator. However, a period of temporal overlap between the deposition and etching phases exists due to the finite time responses of the mass flow controllers (MFC). For each cycle k in Eq. (A3), half of this overlap period has been included in T_k^D, and the other half is included in T_k^E. During the etching phase, it is assumed that the etching of silicon starts *after* the passivation layer at the bottom of the trench has been etched completely. The time spent on etching the passivation layer may not necessarily be the same for every cycle due to the fact that the rates of both fluorocarbon polymer deposition and etching are aspect ratio dependent. As such, the time spent on etching the passivation layer *cannot* be controlled by the operator. For the kth cycle, one can assume a more general expression where these times are variable, or

$$T_k^E = T_k^{E,P} + T_k^{E,S}, \tag{A4}$$

where $T_k^{E,P}$ is the time elapsed during the passivation layer etch of the kth cycle, and $T_k^{E,S}$ is the time elapsed during the silicon etch of the kth cycle. Since the passivation layer at the bottom of the trench must be removed before silicon etching can proceed, the relationship between $T_k^{E,P}$ and T_k^D can be expressed as

$$T_k^D D_k = T_k^{E,P} E_k^P = Y_k, \tag{A5}$$

where D_k and E_k^P are the aspect ratio dependent deposition rate and etch rate of the fluorocarbon polymer passivation layer during cycle number k, respectively, previously cited in Eqs. (1) and (9). Discussions of $D_k(a)$ and $E_k^P(a)$ are included in Sec. II. Y_k is the thickness of the passivation layer for the

kth cycle. Now, define H_k as the incremental silicon etch progression achieved during cycle number k, or

$$H_k = T_k^{E,S} E_k^S, \tag{A6}$$

where E_k^S is the aspect ratio dependent etch rate of silicon during the kth cycle, previously cited in Eq. (8).

In the above analysis, D_k, E_k^P, and E_k^S are assumed to be constant *within* the kth cycle, evaluated at the aspect ratio observed at the beginning of the cycle, a_k. In this manner, we neglect the small rate changes that occur when the aspect ratio increases or decreases during the etch and deposition subprocesses of a given cycle. Strictly speaking, this assumption does not hold for E_k^S during the initial stages of the DRIE of a narrow trench, since the change of aspect ratio during early cycles may be significant. For this reason, the model does not use a cycle by cycle analysis to model the apparent etch rate of trenches up to an aspect ratio of 5. However, since the DRIE cycle period is small, i.e., less than 20 s, and E_k^S decreases as the aspect ratio increases, neglecting deposition/etch rate fluctuations within a given cycle is reasonable for the large majority of etching cycles that begin with $a_k > 5$. Specifically, for a given trench width, 2 μm $< w < 50$ μm, and $a_k \geqslant 5$, the aspect ratio will change by less than 10% during progression of the cycle resulting in only small deviations in instantaneous etch rate. With this assumption, the instantaneous etch rate of the DRIE process for cycle number k can be estimated as

$$E_k^{ins} = \frac{H_k}{T_k}. \tag{A7}$$

Substituting from Eqs. (A4)–(A7), we have

$$E_k^{ins} = \frac{H_k}{T_k} = \frac{E_k^S}{T_k^E + T_k^D}\left(T_k^E - \frac{T_k^D D_k}{E_k^P}\right) = \frac{E_k^S}{1 + \beta_k}\left(1 - \frac{\beta^k D_k}{E_k^P}\right), \tag{A8}$$

where β_k is defined as time ratio between deposition and etching phases for the kth cycle, or

$$\beta_k = \frac{T_k^D}{T_k^E}. \tag{A9}$$

The total etched depth, h, can now be written as

$$h = h_{initial} + \sum_{k=1}^{n} H_k = h_{initial} + \sum_{k=1}^{n}\left(T_k^E - \frac{T_k^D D_k}{E_k^P}\right)E_k^S. \tag{A10}$$

If T_k^D and T_k^E are held constant for all n cycles of the DRIE process, then $T_k^D = T^D$, $T_k^E = T^E$, and $\beta_k = \beta$. Substituting Eq. (A3) and Eq. (A10) into Eq. (A2) gives the apparent etch rate,

$$E_n = \frac{h_{initial} + \sum_{k=1}^{n} H_k}{t_{initial} + \sum_{k=1}^{n} T_k} = \frac{h_{initial} + T^E \sum_{k=1}^{n}\left(1 - \frac{\beta D_k}{E_k^P}\right)E_k^S}{t_{initial} + nT^E(1 + \beta)}. \tag{A11}$$

[1] M. A. Blauw, T. Zijilstr, and E. van der Drift, J. Vac. Sci. Technol. B **19**, 2930 (2001).
[2] J. Yeom, Y. Wu, and M. A. Shannon, in Proceedings of Transducers '03-The 12th International Conference on Solid State Sensors, Actuators and Microsystems, IEEE, Boston, MA, p. 1631 (2003).
[3] A. A. Ayón, R. Braff, C. C. Lin, H. H. Sawin, and M. A. Schmidt, J. Electrochem. Soc. **146**, 339 (1999).
[4] J. Kiihamaki and S. Franssila, J. Vac. Sci. Technol. A **17**, 2280 (1999).
[5] R. A. Gottscho and C. W. Jurgensen, J. Vac. Sci. Technol. B **10**, 2133 (1992).
[6] M. J. Sowa, M. E. Littau, V. Pohray, and J. L. Cecchi, J. Vac. Sci. Technol. A **18**, 2122 (2000).
[7] C. B. Labelle, V. M. Donnelly, G. R. Bogart, R. L. Opila, and A. Kornblit, J. Vac. Sci. Technol. A **22**, 2500 (2004).
[8] M. Schaepkens, G. S. Oehrlein, and J. M. Cook, J. Vac. Sci. Technol. B **18**, 848 (2000).
[9] J. W. Coburn and H. F. Winters, Appl. Phys. Lett. **55**, 2730 (1989).
[10] T. M. Mayer and R. A. Barker, J. Vac. Sci. Technol. **21**, 757 (1982).
[11] M. A. Blauw, E. van der Drift, G. Marcos, and A. Rhallabi, J. Appl. Phys. **94**, 6311 (2003).
[12] T. E. F. M. Standaert, M. Schaepkens, N. R. Rueger, P. G. M. Sebel, and J. M. Cook, J. Vac. Sci. Technol. A **16**, 239 (1998).
[13] P. Clausing, Ann. Phys. (Paris) **12**, 961 (1932).
[14] B. E. Volland, Tzv. Ivanov, and I. W. Rangelow, J. Vac. Sci. Technol. B **20**, 3111 (2002).
[15] S. Rauf, W. J. Dauksher, S. B. Clemens, and K. H. Smith, J. Vac. Sci. Technol. A **20**, 1177 (2002).
[16] J.-H. Min, G.-R. Lee, J.-K. Lee, and S. H. Moon, J. Vac. Sci. Technol. A **22**, 661 (2004).
[17] F. Ulacia, J. Ignacio, C. J. Petti, and J. P. McVittie, J. Electrochem. Soc. **135**, 1521 (1988).
[18] W. T. Pike, W. J. Karl, S. Kumar, S. Vijendran, and T. Semple, Microelectron. Eng. **73–74**, 340 (2004).
[19] B-O. Cho, S-W. Hwang, G-R. Lee, and S. H. Moon, J. Vac. Sci. Technol. A **19**, 730 (2001).
[20] S. Jensen and O. Hansen, Proc. SPIE **5342**, 111 (2004).
[21] C. Hedlund, H. O. Blom, and S. Berg, J. Vac. Sci. Technol. A **12**, 1962 (1994).
[22] H. Sun, T. Hill, H. Taylor, M. Schmidt, and D. Boning, in Proceedings of MEMS05, IEEE, Miami (2005).
[23] I. W. Rangelow, J. Vac. Sci. Technol. A **21**, 1550 (2003).